ELSEVIER

Physics of the Earth and Planetary Interiors 115 (1999) 147–171

PHYSICS OF THE EARTH AND PLANETARY INTERIORS

www.elsevier.com/locate/pepi

Age and magnetism of lavas in Jökuldalur area, Eastern Iceland: Gilsá event revisited

Saneyuki Udagawa [a], Hajime Kitagawa [b,1], Agust Gudmundsson [c], Osamu Hiroi [b,2], Takehiro Koyaguchi [a], Hidefumi Tanaka [d], Leo Kristjansson [e], Masaru Kono [b,*,3]

[a] *Earthquake Research Institute, University of Tokyo, Bunkyo-ku, Tokyo 113, Japan*
[b] *Department of Earth and Planetary Physics, University of Tokyo, Bunkyo-ku, Tokyo 113, Japan*
[c] *AGUST, Geological Services, Armuli 4, 108 Reykyavik, Iceland*
[d] *Faculty of Education, Kochi University, Kochi-shi, Kochi 780, Japan*
[e] *Science Institute, University of Iceland, Reykjavik, Iceland*

Received 30 April 1998; received in revised form 6 January 1999; accepted 14 March 1999

Abstract

We present results of paleomagnetic measurements and K–Ar age determinations of 38 lava flows collected in five separate sections in the Jökuldalur area of Eastern Iceland, including one section previously studied by Watkins et al. [Watkins, N.D., Kristjansson, L., McDougall, I., 1975. A detailed paleomagnetic survey of the type location for the Gilsá geomagnetic polarity event. Earth Planet. Sci. Lett. 27, 436–444]. These sites are close to the type locality of the normal ''Gilsá event'' in the Matuyama chron first identified by McDougall and Wensink [McDougall, I., Wensink, H., 1966. Paleomagnetism and geochronology of the Pliocene–Pleistocene lavas in Iceland. Earth Planet. Sci. Lett. 1, 232–236]. Using new experimental results as well as field observations, we could correlate the sequence of lava flows in the Jökuldalur area spanning the time interval between 1.8 and 0.5 Ma. The magnetic polarities and ages obtained in this study are quite consistent with the standard time scale for Brunhes–Matuyama ages given by Cande and Kent [Cande, S.C., Kent, D.V., 1995. Revised calibration of the geomagnetic polarity timescale for the Late Cretaceous and Cenozoic. J. Geophys. Res. 100, 6093–6095] based on marine magnetic anomalies, except that the Gilsá event needs to be added. Existence of Olduvai age lavas under Gilsá was inferred but not certain. Our results are fairly in good agreement with the former studies by Wensink [Wensink, H., 1964a. Secular variation of Earth magnetism in Plio–Pleistocene basalts of eastern Iceland. Geol. Mijnbouw 43, 403–413; Wensink, H., 1964b. Paleomagnetic stratigraphy of younger basalts and intercalated Plio–Pleistocene tillites in Iceland. Geol. Rund. 54, 364–384] and Watkins et al. [Watkins, N.D., Kristjansson, L., McDougall, I., 1975. A detailed paleomagnetic survey of the type location for the Gilsá geomagnetic polarity event. Earth Planet. Sci. Lett. 27, 436–444], but the assignment to the polarity zones is different because of the newly obtained K–Ar ages. Based on the present study,

* Corresponding author. Tel.: +81-858-43-3829; fax: +81-858-43-2184; E-mail: mkono@misasa.okayama-u.ac.jp
[1] Now at the Patent Agency, Ministry of International Trade and Industries.
[2] Now at Kita-Kamakura Girls High School.
[3] Now at Institute for Study of the Earth's Interior, Okayama University.

PII: S0031-9201(99)00073-4

we propose that the Gilsá event is a short normal subchron in the Matuyama chron distinct from and above the more well-established Oldvai subchron.

Keywords: Magnetism; Lava; Gilsá event

1. Introduction

Detailed paleomagnetic study of lava flows in the Jökuldalur valley in Eastern Iceland was originally carried out by Wensink (1964a,b). In his first paper, Wensink (1964a) reported paleomagnetic results from 17 lava flows in Jökuldalur obtained by laboratory treatment including alternating field (AF) demagnetization. In the second paper, Wensink (1964b) extended the polarity correlation not only to the upstream part of Jökuldalur but also to Hofsardalur to the north and Fljotsdalur to the south, using mostly measurements by magnetic compass to determine the polarity of the remanence in the field. By these correlations, Wensink established the stratigraphy covering the polarity zones of N_1 (which corresponds to Brunhes epoch or chron), R_1 (Matuyama), N_2 (Gauss), and R_2 (Gilbert) in this area. In these studies, Wensink noted that up to three normal lavas are found in the middle of the thick reversed sequence of R_1.

Subsequently, the R_1 and N_2 lavas were dated by McDougall and Wensink (1966) by K–Ar method. Because the age they obtained for the normal lava flow (No. 17 in Wensink's numbering) in the R_1 sequence (1.61 ± 0.05 Ma, using the new decay constants of Steiger and Jäger, 1977) was somewhat younger than that of the Olduvai event (subchron) originally reported by Grommé and Hay (1963) (also Grommé and Hay, 1967, 1971), McDougall and Wensink (1966) suggested that this represents a new polarity episode in the Matuyama epoch (chron) which they called the Gilsá event (subchron). Existence of a lava recording the Olduvai event was suggested from the observation of Wensink (1964a,b) who found a reversed lava sandwiched between two normal lavas (his 16 and 17, but Wensink placed a question mark to this polarity in his figure).

Paleomagnetic and age results of the Gilsá event were reconfirmed by a detailed study of the type locality (GH and GL sections in Fig. 1) by Watkins et al. (1975). However, they could not find the reversed flow which McDougall and Wensink described to exist between the lavas 16 and 17. Moreover, the dates obtained for these two lavas were not significantly different from each other. Their preferred age of the two normal lavas was 1.62 ± 0.02 Ma (with new decay constants). Consequently, they denied the existence of a separate normal period below Gilsá lavas, which the former studies suggested to belong to Olduvai. The distinction between Olduvai and Gilsá was not made clear by this study.

Following these studies, Gilsá event (subchron) was included in some of the earlier geomagnetic polarity time scales (GPTS, e.g., Cox et al., 1968; Cox, 1969a; McDougall, 1979). However, more recent standard scales (e.g., Cande and Kent, 1992, 1995) do not contain Gilsá event as one of the subchrons in the Matuyama chron. This perhaps reflects the fact that these time scales rely more and more on good quality oceanic magnetic anomaly data rather than dated subaerial lava flows. Although magnetic anomaly data are ideal in supplying homogeneous data which are nearly continuous in time, they also have shortcomings that very short reversal episodes cannot be distinguished because of the problem of resolution.

Even if Gilsá is too short to be identified in the marine magnetic data, it is still interesting to see if this is a true magnetic reversal phenomenon. How often short reversals occur depends critically on the stability of the magnetic field generation and its

Fig. 1. Sampling sites in the Jökuldalur area in Eastern Iceland. Lava flows sampled in this study are indicated by dots, and the sections studied by Watkins et al. (1975) are shown by thick lines. KG section is the same as the GK section of Watkins et al. The possible continuation of Gilsá age lavas is indicated based on the studies of Wensink (1964b) and Watkins et al. (1975) for GL and GH, and our results for KG and BD sections. Thin continuous lines are the rivers and tributaries, while dashed lines show contour lines at 100-m intervals.

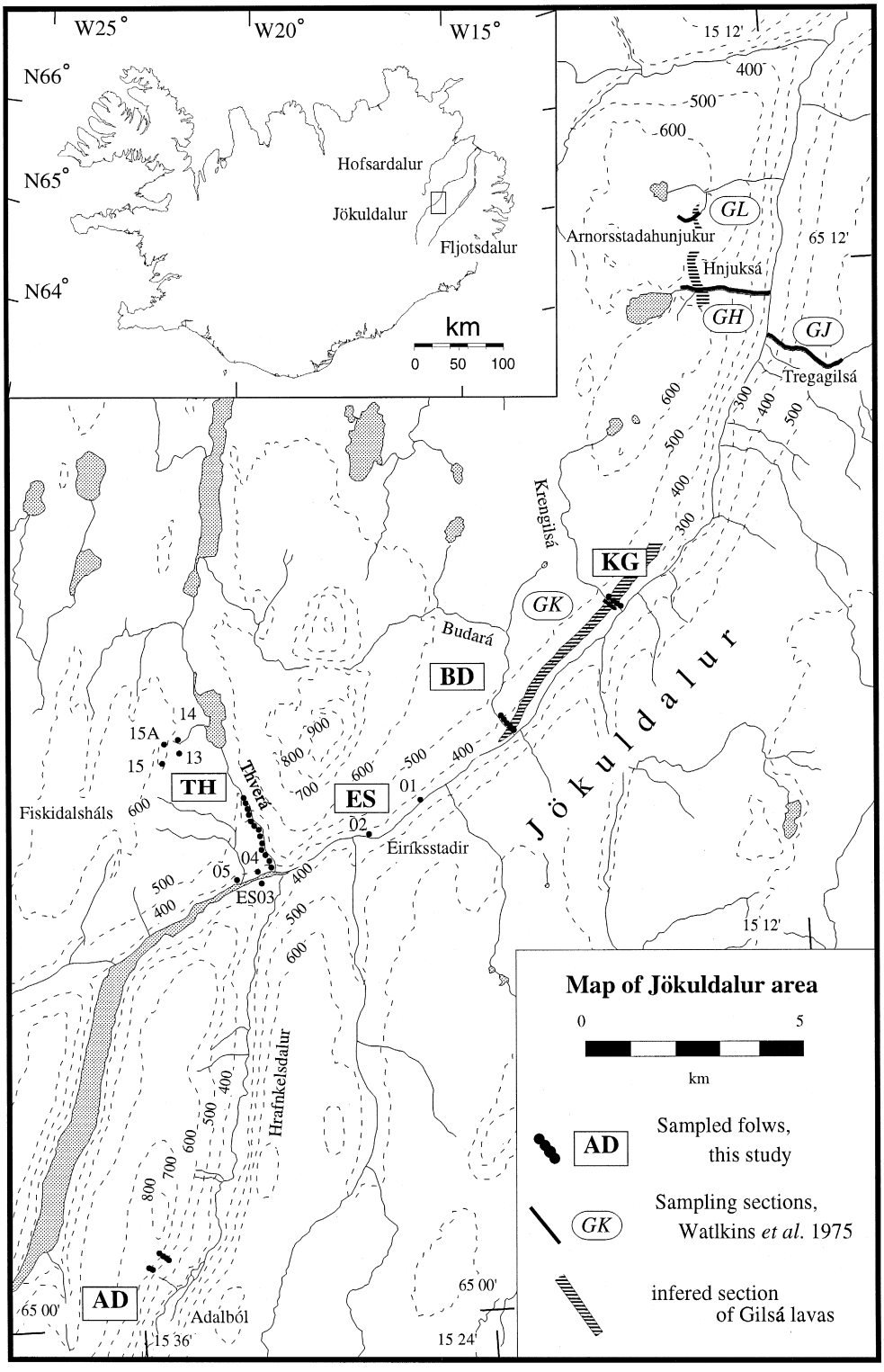
W25°
W20°
W15°
N66°
N65°
N64°
Hofsardalur
Jökuldalur
Fljotsdalur
km
0 50 100
15 12'
400
500
600
GL
Arnorsstadahunjukur
65 12'
Hnjuksá
GH
GJ
Tregagilsá
Krengilsá
KG
GK
Budará
BD
Jökuldalur
14
15A
13
15
TH
Fiskidalsháls
Thverá
ES
01
02
Eiríksstadir
04
05
ES03
Hrafnkelsdalur
AD
Adalból
65 00'
15 36'
15 24'
Map of Jökuldalur area
0 5
km
Sampled folws, this study
Sampling sections, Watlkins et al. 1975
infered section of Gilsá lavas

maintenance, and thus, may be quite important in considering the working mechanism of the geodynamo. In addition, short reversals of the magnetic field proved quite useful in stratigraphic correlation, because they can be used as very good time markers. In the recent years, accumulation of high quality paleomagnetic data, as well as biostratigraphic and isotopic data, have made it possible to carry out a remarkably detailed correlations (e.g., Hilgen, 1991; Zijderveld et al., 1991). It thus seems important to repeat paleomagnetic works in this area using the more sophisticated techniques of paleomagnetism and age dating of today.

In 1993 and 1994, we carried out sampling of lava sequences in the Jökuldalur area in Eastern Iceland. These included the lavas which were measured by Watkins et al. (1975) in their study of Gilsá event lavas. Careful field studies in the line of work of Wensink (1964a,b), together with the K–Ar ages obtained in this study, made it possible to correlate them for a time sequence of 0.5 to 2 Ma. In this paper, we describe stratigraphy, paleomagnetic measurements, and K–Ar age determination results obtained from this area, and argue that Gilsá event is a short normal subchron younger than and distinct from the well-established Olduvai subchron.

2. Geology and sampling

The area of sampling is located about 50 km east of the North Iceland Rift Zone, which is the center of the present-day volcanism, and consists of volcanic rocks of ages 3.1 Ma or younger, including Quaternary glacial periods (Fig. 1). In ice ages, magma erupted under the ice sheet forming flat-topped table mountains which consist of hyaloclastites. In interglacial periods, lavas flowed down and buried the valleys between these topographically high hyaloclastite hills. In some cases, it is possible that lavas found at low valleys are stratigraphically higher than the hyaloclastites at the top of the hills. We tried to reconstruct the landforms at the time of lava eruption in order to obtain the correct stratigraphic correlations between different units. We also took into account the general dip of the lava flows in this area. The stratigraphic correlation we obtained by these methods seems to be generally supported by the K–Ar ages from these rocks as shown later.

The sampling localities are shown in Fig. 1. Samples were collected along small tributaries joining in the Jökuldalur from NNW direction, namely, Krengilsá (KG), Budará (BD), and Thverá (TH), in the river bed of Jökuldalur itself near Eiriksstadir (ES), and at Adalbol (AD) along Hrafnkelsdalur which flows from south and joins the Jökuldalur. The stratigraphic relations between the sampled lavas are shown in Fig. 2. In the sampled sections, lavas were usually numbered from low to high altitudes. But some departure from this scheme was inevitable, because we were often obliged to change the sampling plan based on field observations.

Six core samples of 25 mm diameter were drilled at each site by a portable engine drill. Five cores were oriented in situ, using the direction of the sun, reference marks identifiable on maps, and/or magnetic compass. The sixth core was unoriented because that was collected for the use in dating and chemical analyses. Where possible, samples were drilled at least 2 m apart to cancel the effect of very localized magnetic anomalies. The following gives the descriptions of individual sampling sites.

2.1. KG section

This section is exposed along the lower part of KG tributary and is exactly the same as the GK section of Watkins et al. (1975). The flows sampled by them could easily be identified by the existence of drill holes. We sampled four basalt lavas in this section. The lowest unit (KG00A) was taken from the massive lava block (larger than a few meters across) emplaced in a hyaloclastite layer just below a small bridge near the confluence with the main stream. This layer was not sampled by Watkins et al. (1975). Among the other three units, the lower two (KG00 and KG01) were from the normal part (GK2 and GK4 of Watkins et al.) and the topmost one (KG02) was from the reversed part of the sequence (GK9 of Watkins et al.).

2.2. BD section

The small valley of the stream BD is located between the KG section and the TH section tribu-

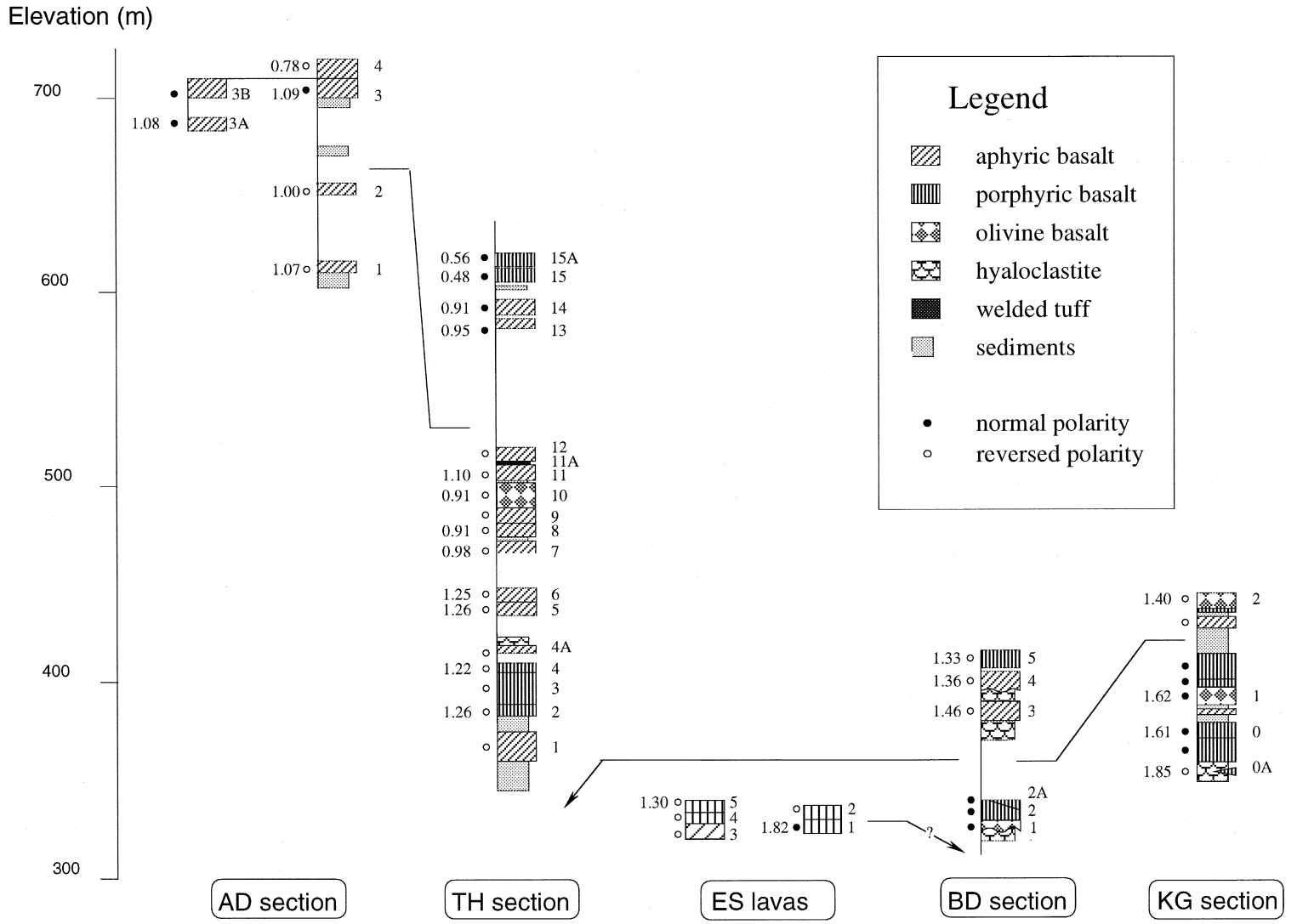

Fig. 2. Stratigraphic correlation of lava flows sampled in Jökuldalur area. Flow numbers and the K–Ar ages determined for selected lavas are shown on the right and left of each section. Elevation is above the mean sea level. Part of the paleomagnetic polarities shown for KG section are based on Watkins et al. (1975). Possible stratigraphic correlations are indicated by lines.

taries. Six lava flows were sampled. At the topographically lowest point, plagioclase basalts (BD01, BD02, BD02A) overlie a hyaloclastite layer. At a higher position, aphyric basalt (BD03) is found overlying another hyaloclastite layer.

2.3. ES flows

These are sampled along the river bed of Jökuldalur near Eiriksstadir. Thus, all of them lie at a height of about 330 m. Stratigraphic relations are not very clear, but since this area generally dips about 1° to 2° toward west, ES01 and 02 must be older than ES03–ES05. ES03–ES05 lavas were sampled close to the confluence of TH and therefore, seem to correspond to the lowermost part of the TH section.

2.4. TH section

This section is underlain by a sediment layer which contains abundant quenched lava fragments. Another thin layer of hyaloclastite appears just above TH04A. In this section, TH01 through TH12 were sampled along the valley of the TH tributary where lavas form a continuous succession. On the other hand, TH13, 14, 15, and 15A were sampled on the topmost parts of Fiskidalsháls hill, and the stratigraphic relation is less clear. Between TH14 and TH15 (and TH15A), there is a layer of conglomerate suggesting a considerable time gap between these two lavas.

2.5. AD section

Here, the height is similar to that of the TH section, but this section is characterized by the abundance of sediments. The lowest part is especially dominated by sedimentary layers and hyaloclastites. The lavas AD01 and AD02 are interbedded at intervals in this zone. The lava AD03B is similar in height as AD03, but was sampled about 1 km to the southwest. AD03A is just below AD03B and should fill in the gap between AD03 and AD02.

3. Paleomagnetism

Cylindrical specimens with a diameter of 25 mm and a length of 22 mm were cut from the oriented cores, and one specimen from each core was used in paleomagnetic experiments. After the measurement of the NRM, all of these specimens (except AD series) were subjected to 10 steps of AF demagnetization at 5 mT intervals, i.e., 5, 10, ..., 50 mT. Specimens from AD series were demagnetized in five steps of 10 mT intervals to 50 mT. Such detailed treatments became possible by the use of a newly developed automatic spinner magnetometer-AF demagnetizer system, which can complete the measurement for one specimen (11 measurements and 10 demagnetization steps in the above treatment) in about 10 min. The spinner magnetometer part of this system is based on the concept described by Kono et al. (1984). Integration of the AF demagnetizer into the system was reported by Kono et al. (1997).

As is common with most basaltic lavas in Iceland, the main magnetic carriers in our samples are titanomagnetite or magnetite. Magnetites are probably the products of high-temperature oxidation while lavas were cooled from melting temperature (Larson et al., 1969). Magnetic minerals are found in either single domain (SD) or pseudo-single domain (PSD) state (Day et al., 1977). Results of rock magnetic experiments are summarized in Appendix A.

3.1. Results of AF demagnetization

Nearly all the specimens showed a good behavior in stepwise AF demagnetization. Typical examples of AF demagnetization results are shown in Fig. 3. In the first two examples, (a) directions of remanences did not change at all (KG00-4-3), or (b) some apparent overprint could be removed by demagnetization at a very low field such as 5 or 10 mT, after which only a single component remains (BD04-5-3). In these examples, (nearly) all of the points lie on a straight line, showing that these NRMs consist of a

Fig. 3. Examples of changes in the remanent magnetization during stepwise AF demagnetization. (a)–(d) are orthogonal plots showing the decay of remanence in AF demagnetization at 5-mT intervals to 50 mT. Closed and open circles represent projections to horizontal and vertical planes, respectively. (e) and (f) show changes in the direction of remanence in demagnetization. Note that for the case of TH14-2-1, the ChRM direction was not reached and only the great circle was defined.

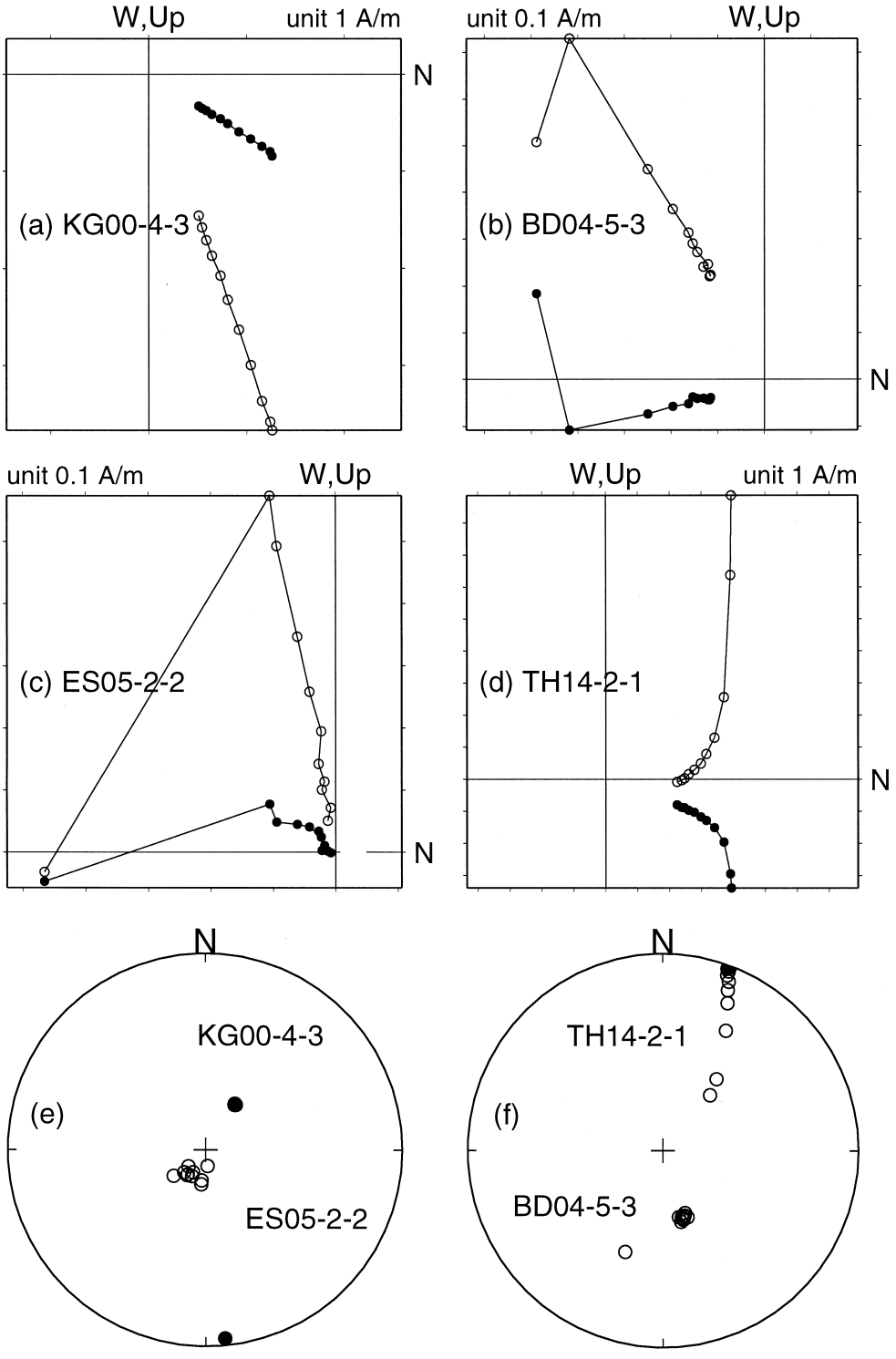
W,Up
unit 1 A/m
N
(a) KG00-4-3
unit 0.1 A/m
W,Up
(b) BD04-5-3
N
unit 0.1 A/m
W,Up
(c) ES05-2-2
N
W,Up
unit 1 A/m
(d) TH14-2-1
N
N
KG00-4-3
(e)
ES05-2-2
N
TH14-2-1
(f)
BD04-5-3

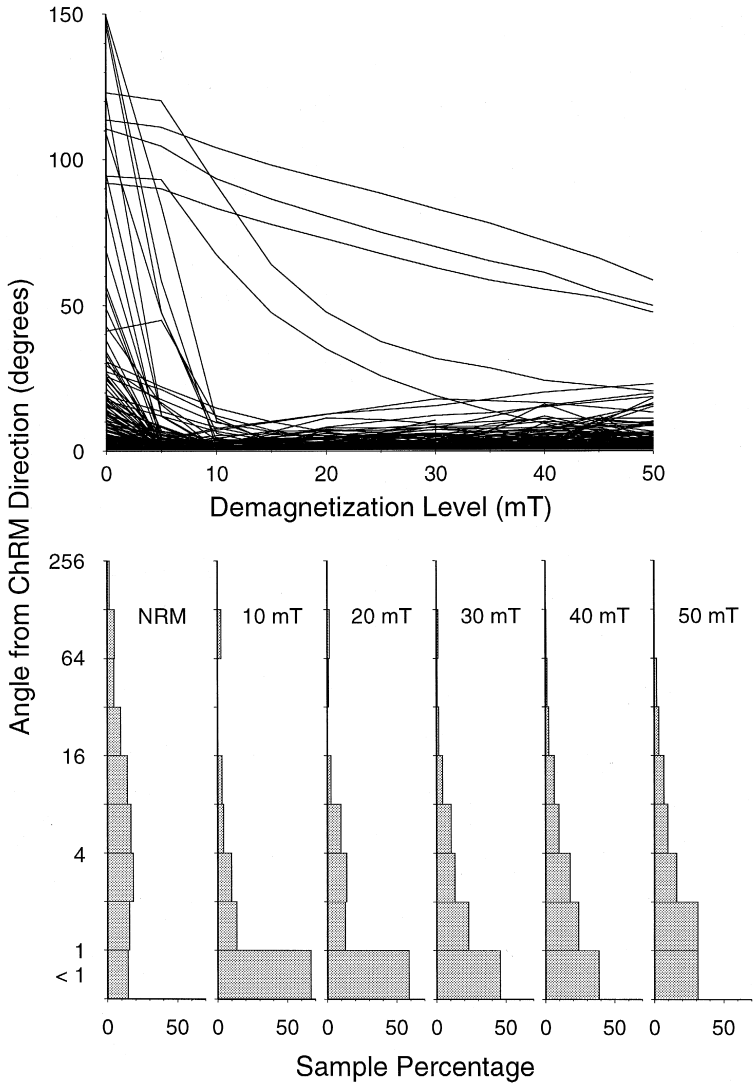

Fig. 4. Approach to the direction of ChRM. Top: Change in each specimen of angular difference from the ChRM direction at each demagnetization step (linear scale). Bottom: Histograms of angular difference at various steps (logarithmic scale).

single component characteristic remanent magnetization (ChRM). In some others, (c) the primary component cannot be recovered at such low fields, but orthogonal diagrams showed a distinct ChRM starting from about 25 or 30 mT (ES05-2-2). The 10-point AF demagnetization scheme employed in the present study can reliably determine the primary magnetization direction in most samples as these examples

Fig. 5. The most complicated of demagnetization (TH13). The ordinary principal component analysis gives widely different directions (a), but good convergence was attained (j) with the application of combined analysis of directions and remagnetization planes of McFadden and McElhinny (1988). (b) to (f) show the orthogonal plots for individual samples, (k) and (l) are about 10 × blow-ups of (e) and (f), and (g) to (i) show the direction changes and the sector constrained great circles for three of the samples.

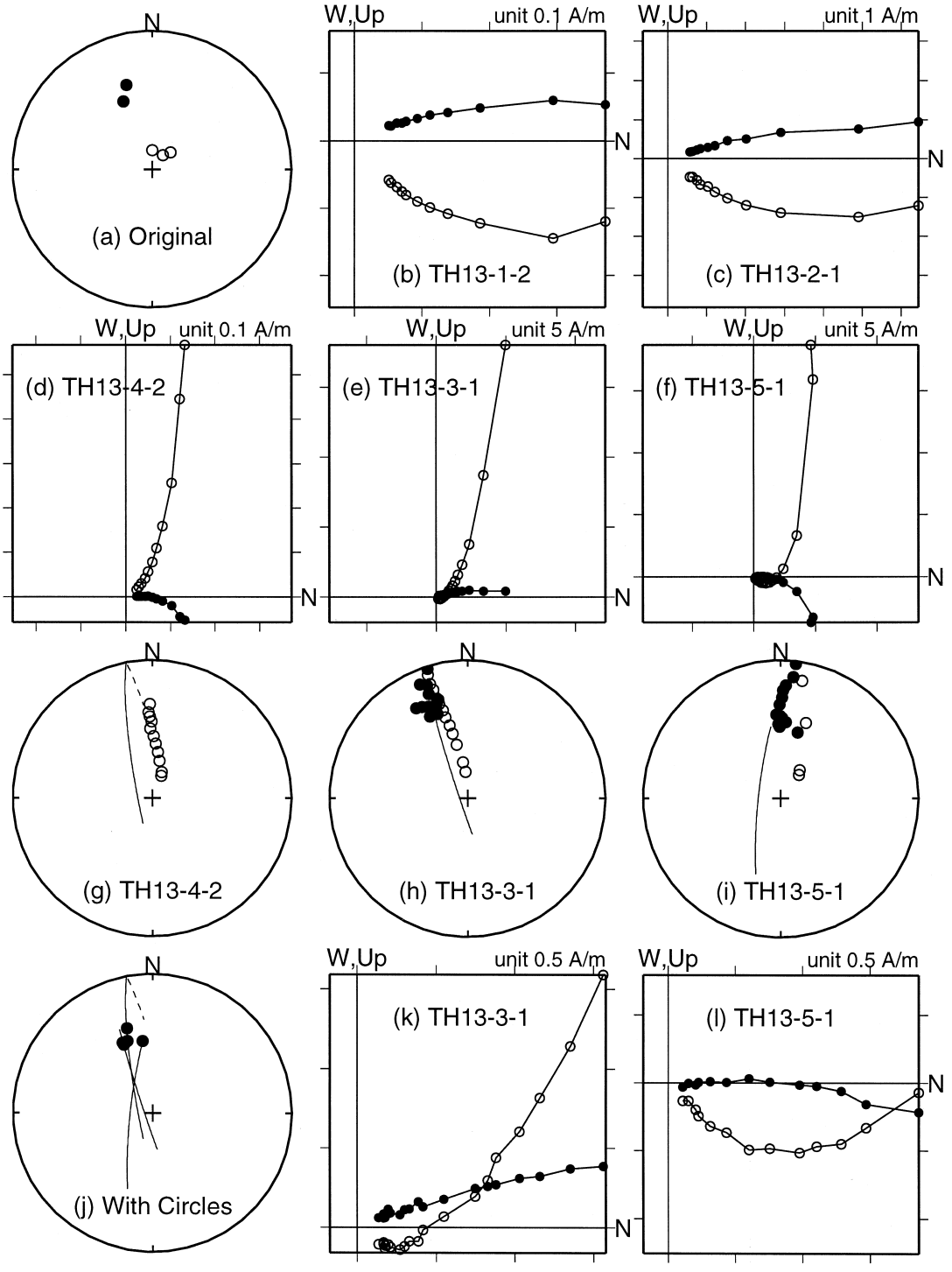
N
(a) Original
W,Up
unit 0.1 A/m
N
(b) TH13-1-2
W,Up
unit 1 A/m
N
(c) TH13-2-1
W,Up
unit 0.1 A/m
(d) TH13-4-2
N
W,Up
unit 5 A/m
(e) TH13-3-1
N
W,Up
unit 5 A/m
(f) TH13-5-1
N
N
(g) TH13-4-2
N
(h) TH13-3-1
N
(i) TH13-5-1
N
(j) With Circles
W,Up
unit 0.5 A/m
(k) TH13-3-1
N
W,Up
unit 0.5 A/m
(l) TH13-5-1
N

Table 1
Paleomagnetic directions and poles from Jökuldalur basalts
Height: height above sea level; N: total number of samples (number in parentheses indicate the samples for which the method of remagnetization circle was used); I, D: mean inclination and declination; R: length of N unit vectors directed to mean directions; α_{95}: semi-angle of 95% confidence; k: precision parameter of Fisher (1953); λ_p, ϕ_p: VGP latitude and longitude.

Lava	Height (m)	N	I (°)	D (°)	R	α_{95} (°)	k	λ_p (°N)	ϕ_p (°E)
AD section									
AD04	708	5	−70.3	−46.0	4.9801	5.4	201	−34.5	−169.5
AD03	698	5	68.5	77.8	4.9909	3.6	441	50.1	50.6
AD03B	698	5	75.3	−22.3	4.9940	3.0	662	79.8	−115.0
AD03A	680	5	82.3	44.7	4.9648	7.2	113	72.4	17.5
AD02	646	5	−76.3	−137.3	4.9946	2.8	737	−72.0	−126.6
AD01	606	5	−67.1	165.9	4.9820	5.2	221	−73.1	12.9
TH section									
TH15A	609	5	74.8	−43.0	4.9947	2.8	748	70.7	−100.5
TH15	609	5	67.6	−59.6	4.9874	4.3	317	56.6	−106.5
TH14	592	5 (2)	60.3	−12.0	4.9757	6.0	164	65.3	−178.1
TH13	584	5 (3)	44.5	−14.8	4.9626	7.4	107	50.0	−179.1
TH12	516	5	−62.3	−167.5	4.9802	5.4	202	−67.5	−44.1
TH11A	509	5	−61.2	173.1	4.9897	3.9	389	−67.0	−6.8
TH11	504	5	−58.3	−160.1	4.9678	6.9	124	−61.5	−53.7
TH10	493	5	−68.8	161.9	4.9945	2.8	730	−74.2	24.3
TH09	482	5	−72.6	171.1	4.9879	4.2	331	−81.8	14.9
TH08	475	5	−78.8	173.1	4.9878	4.2	327	−85.7	123.5
TH07	466	5	−69.8	163.5	4.9799	5.4	199	−75.9	23.9
TH06	456	5	−64.2	−169.0	4.9929	3.2	560	−70.1	−42.8
TH05	449	5	−66.8	167.5	4.9958	2.5	944	−73.1	9.1
TH04	408	5	−88.3	79.6	4.9835	4.9	242	−64.2	152.4
TH03	397	5	−81.0	−159.0	4.9972	2.0	1435	−79.4	−164.0
TH02	386	5	−85.6	161.5	4.9903	3.8	414	−73.0	150.6
TH01	368	5	−75.5	−161.3	4.9866	4.4	298	−81.5	−103.0
ES lavas									
ES05	330	5	−81.5	−148.7	4.9820	5.1	222	−76.4	−160.7
ES04	330	5	−80.8	−129.8	4.9928	3.3	555	−71.0	−153.2
ES03	330	5	−68.8	−145.9	4.9866	4.4	299	−68.5	−89.7
ES02	330	5	−66.4	163.3	4.9963	2.3	1095	−71.6	16.9
ES01	330	5	66.3	25.5	4.9942	2.9	689	68.9	108.0
BD section									
BD05	411	5	−57.8	162.0	4.9861	4.5	287	−61.4	10.4
BD04	399	5	−59.1	178.3	4.9889	4.0	358	−64.8	−17.0
BD03	384	5	−80.9	−179.9	4.9919	3.4	493	−82.8	160.3
BD02A	343	6	85.3	115.8	5.9921	2.7	632	59.9	−3.2
BD02	338	5	86.6	−135.1	4.9961	2.4	1033	59.8	−29.6
BD01	330	5	87.5	−55.4	4.9890	4.0	363	67.5	−30.7
KG section									
KG02	440	5	−59.4	154.4	4.9881	4.2	336	−61.2	23.3
KG01	392	5	81.8	8.6	4.9958	2.5	948	80.6	−5.3
KG00	374	5	66.7	29.5	4.9954	2.6	878	67.9	101.3
KG00A	353	5	−61.2	167.4	4.9782	5.7	183	−66.2	3.5

show. In the cases (a)–(c), a straight line can be fitted to the higher AF steps with good confidence, and there is no ambiguity in the determination of the ChRM as can also be appreciated from the clustering of the directions in equal area projections (Fig. 3e and f). The ChRM directions of these samples were calculated by the method of principal component analysis of Kirschvink (1980).

The diagram for TH14-2-1 (Fig. 3d) shows an example in which the secondary component cannot completely be removed in low AFs such as 50 mT. The trajectory of the remanence in the orthogonal plot is curved and the direction of magnetization moved on a great circle (Fig. 3f) indicating that it gradually approached toward the direction of the primary component. In such cases, (d) the end points of the AF demagnetization or the straight lines fitted to the points may not give the direction of the ChRM.

Among the 191 specimens from 38 flow units subjected to stepwise AF demagnetization, those belonging to (a) and (b) form a clear majority of about 90%. Specimens of (c) and (d) categories are only about 10% and less than 2%, respectively. This somewhat qualitative statement is quantified in Fig. 4, which shows the change in the angle of deflection from the ChRM directions calculated for each sample. The NRM directions may be quite different from that of the ChRM, but directions within 4° of the ChRM can be obtained in more than 90% of the samples after demagnetization to only 10 mT. These samples can be classified as either (a) or (b). If we make the tolerance of 8°, most of the rest of the samples reach the ChRM directions by demagnetization to 20 or 30 mT.

Exceptions to the above conclusion were found only in two flows TH13 (Fig. 5) and TH14 (Fig. 3f). For these lavas, widely different ChRM directions were obtained if we apply the principal component analysis method of Kirschvink (1980) in a direct way (Fig. 5a). Examination of individual orthogonal plots indicate that some of the samples show rather well-defined normal (north and downward) directions (Fig. 5b and c), while others gave steep upward directions in low field demagnetization steps (Fig. 5d–f and Fig. 3d). For some of these samples, AF demagnetization was continued to 200 mT. The blow-up of the high field portion of the orthogonal plots (Fig. 5k and l) shows that these remanences eventually became downward pointing, with several points at the high end defining a good linear portion in one

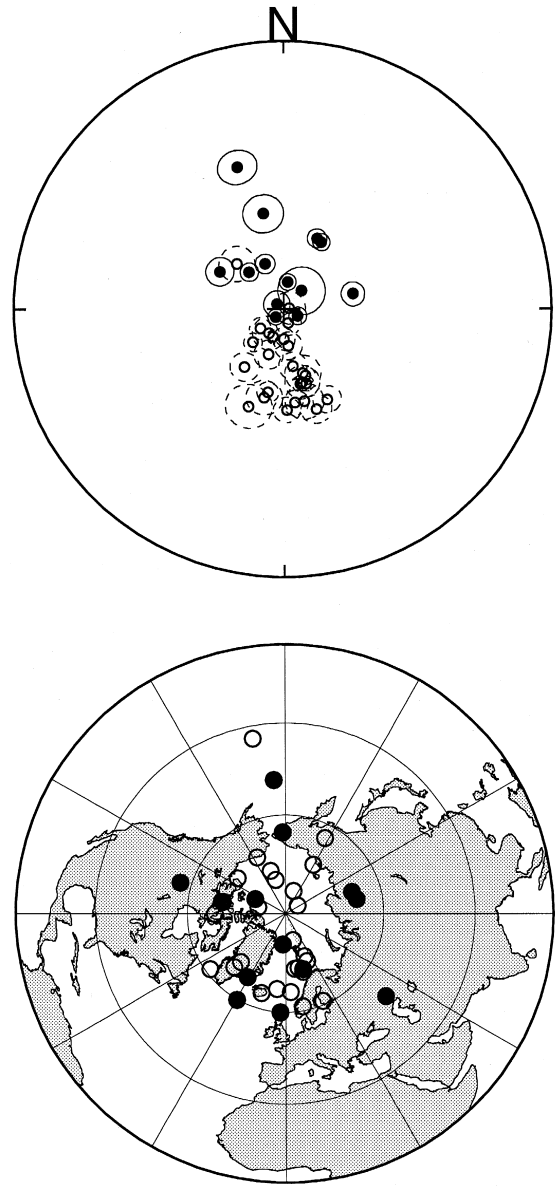

Fig. 6. The mean direction of magnetization of each lava flow with 95% confidence limits (α_{95}) (top), and the distribution of the VGPs corresponding to mean directions (bottom). Closed and open circles correspond to the normal and reverse polarity directions and poles.

example (Fig. 5l), but not such a good linear trend in the other (Fig. 5k).

For these samples, it was possible to use the high-AF portion of orthogonal plot (Fig. 5k and l) to determine the ChRM directions. However, large errors will be incurred by this method since the points are somewhat scattered because the intensity is quite low after AF demagnetization of about 100 mT. We therefore used the combined analysis of directions and great circles of McFadden and McElhinny (1988) to obtain the best estimates of the ChRM directions from these samples. Fig. 5g–i show the remanence directions at various AF steps, as well as the portion of the great circle determined with the sector constraints of McFadden and McElhinny (1988). The combined analysis gives beautiful convergence both for TH13 and TH14. The existence of fixed points (two for TH13 and 3 for TH14), as well as the tight clustering of the final directions (Fig. 5j) show that the method worked remarkably well. Note that for this example, the three great circles almost converge at one point, but that is quite different from the final directions determined with the addition of the fixed points (Fig. 5g).

The reason why only the flows TH13 and TH14 showed such complicated behaviors may be attributed to their mode of exposure. Whereas most of the flows in this study were sampled at fresh outcrops exposed by the activities of rivers or glaciers, these two flows (as well as TH15 and TH15A) were drilled at the top part of a gentle hill. Thus, they have larger possibility of being contaminated, say, by lightning strikes or being affected by local weathering effects compared with the newly cut flows. However, serious mineralogical alterations were not detected even for these flows by examination of thin sections.

3.2. Mean magnetization directions and corresponding poles

In the present study, the worst-behaved flows in terms of ChRM directions are TH13 and TH14, but reliable directions were obtained quite unambiguously even for these after careful treatments as described before (Fig. 5). Thus, AF demagnetization was enough to determine the ChRM directions for all the flows. The mean directions of magnetization of individual lavas are summarized in Table 1. It is to be noted that each mean direction is determined with a very small angle of α_{95}. This is firstly because the rocks are quite well-behaved, but it can also be stressed that the use of the new spinner magnetometer–demagnetizer system helped reduce the measurement errors by eliminating the need to replace the sample between demagnetization and measurements.

Although Watkins et al. (1975) report the paleomagnetic data ''corrected for slight regional dip'' (exact angles were not specified), we did not apply bedding correction to these data. This is because the regional slope observed (1° to 2° toward west) is too small and to appreciably affect the directions even if corrections were applied. Einarsson (1973) noted that the regional dip is about 6° north of the Gilsá type locality, but becomes smaller toward SW along the Jökuldalur valley. Compared to the sites of Watkins et al. (1975), our sites are in areas where the dip is negligibly small.

Table 1 also shows the virtual geomagnetic poles (VGPs) corresponding to the mean direction. The

Table 2
Mean poles and angular standard deviation data
N: number of lava flows; Λ, Φ: latitude and longitude of the mean pole; *R*: length of *N* unit vectors; A_{95}: semi-angle of 95% confidence; *K*: precision parameter; ASD: angular standard deviation of poles and 95% confidence interval. Confidence limits are calculated following Cox (1969b). One reverse flow (AD04) was excluded because of low latitude VGP ($|\Lambda| < 45°$).

Polarity	*N*	Λ (°)	Φ (°)	*R*	A_{95} (°)	*K*	ASD (°)	95% confidence limits (°)
Normal	13	87.0	−16.2	11.6750	14.6	9.1	27.3	21.7–36.9
Reverse	24	−82.7	−13.7	22.8149	6.9	19.4	18.5	15.5–23.0
All	37	86.2	167.0	34.3669	6.6	13.7	22.1	19.1–26.3

distributions of the mean magnetic directions, as well as that of the VGPs, are shown in Fig. 6. It can be seen that the VGPs distribute around the North Pole; i.e., there is no indication of the far-sided effect first pointed out by Wilson (1970). In fact, the geographic pole is well within the 95% circle of confidence (A_{95}) of the mean pole for normal polarity lavas as well as that for both polarities, it is marginally different from the mean pole for reversed polarity (Table 2). The angular standard deviation (ASD) of all the poles (except AD04) is 22.1°, which is slightly smaller than the value of 28° from Iceland summarized for the period of 1.5 to 7 Ma (Kristjansson and Johannesson, 1989) but is not significantly different at the 95% level (Cox, 1969b). It can also be fitted to the global trend comfortably (e.g., Merrill and McElhinny, 1977).

4. K–Ar dating

Samples used in K–Ar analyses were selected by the examination of thin sections prepared from each lava flow. The criteria used for choosing suitable samples was: (1) fresh rocks showing little alteration, and (2) holocrystalline rocks or those which may contain glasses but only between grains. The first condition was to exclude the possibility of secondary movement of K and Ar, while the second condition was to avoid samples which were not in equilibrium with atmospheric Ar, as well as which are susceptible to the loss of K or Ar since the time of eruption. To see the effect of alteration on K–Ar dating, we intentionally included some samples which violates the above selection criteria (see later). It can be seen from the comparison of the results that the criteria employed were quite adequate and reliable ages were obtained from samples satisfying the above conditions.

The samples were crushed and only the central parts of the cores were used in the analyses. They were cleaned ultrasonically in acetone and distilled water, and further crushed with pestle and mortar to 45–80 mesh size. Phenocrysts and magnetic minerals were removed by hand picking and then by magnetic separation to increase the K and Ar contents as well as to avoid contamination due to excess Ar.

4.1. Argon analysis

From the samples prepared in the above procedures, 300 to 400 mg were used for Ar analysis. The samples were cleaned by washing in ethanol and distilled water, and dried at 105°C for 12 h. The samples were then weighed and wrapped in aluminum foil and put in a mass spectrometry system at the Institute for Study of the Earth's Interior (ISEI), Okayama University. This system is composed of standard gas reservoirs, furnace purification line and a mass spectrometer (modified VG5400) which has the mass resolution ($M/\Delta M$) of 800 (Nagao et al., 1996).

The furnace, the purification line, and the samples were baked at 1700, 250, and 200°C, respectively, to lower the background level and to remove the atmospheric gas adsorbed on the surfacial areas of the sample. After these pre-treatments, each sample was introduced in the furnace and melted at 1600°C. The extracted gas was purified by Ti–Zr getters and SORB-AC getters, and spike ^{38}Ar was mixed with the sample gas. After purification, Ar gas of less than 2×10^{-7} Torr was measured by the mass spectrometer.

4.2. Potassium analysis

The remainder of the samples were further ground with pestle and mortar, from which 40–120 mg was dried at 105°C and weighed. The powder sample was dissolved with $HClO_4$ and HF in a teflon beaker and heated for 24 h until it was completely dry. The sample was then dissolved in 1 ml of 6 N HCl, mixed with an internal standard (5 ml of 200 ppm Li solution), and diluted to 50 ml with distilled water. By this procedure, the K content of a typical sample solution was made to about 4 ppm.

Measurement of K was done by a flame photometer (Kotaki FIP-3M) at the Earthquake Research Institute. Standard solutions with different K contents (0.00, 2.50, 4.00, 5.00, 7.50, 10.00 ppm, respectively) were prepared for calibration. In one set of analysis, sodium in nearly the same concentration as in the sample was added to the standard solutions, in order to compensate for the possible effect of ionization interference.

To confirm the accuracy and estimate the precision of the measurements, JB-2 basalt, which is one

of the reference samples distributed from the Geological Survey of Japan (GSJ), was measured with the same procedure, and the K_2O concentration value of $0.417 \pm 0.002\%$ was obtained from 13 measurements. This value is not significantly different from $0.418 \pm 0.013\%$ which is recommended by the GSJ (Ando et al., 1989), or more recently reported value of $0.42 \pm 0.03\%$ (Terashima et al., 1994).

4.3. Age results

From the measured data, K–Ar ages and their errors (at 1σ) were calculated following the procedures routinely used at ISEI. This mass spectrometer is carefully calibrated by Nagao et al. (1996) in the following way. The isotope ratios of atmospheric argon were measured and adjusted to the standard value of $^{40}Ar/^{36}Ar = 295.5$ and $^{38}Ar/^{36}Ar = 0.188$ (Nier, 1950; also see Ozima and Podosek, 1983, p. 13). The isotope ratio of K was taken as $^{40}K/K = 1.167 \times 10^{-4}$, and the decay constants of ^{40}K to ^{40}Ar and ^{40}Ca as $\lambda_e = 0.581 \times 10^{-10}$ yr^{-1} and $\lambda_\beta = 4.962 \times 10^{-10}$ yr^{-1}, respectively (Steiger and Jäger, 1977). These are the only values assumed, and the rest of the numbers needed in calculation were determined from the measurements. The latter includes the isotope ratios of Ar spike as well as that of the standard sample. The accuracy and precision of age determination is estimated by comparing the amount of radiogenic argon and calculated ages for international standard samples (Flisch, 1982; Samson and Alexander, 1987). Table 3 shows a good consistency between the values obtained at ISEI and the internationally adopted values. Together with the small experimental errors, the reliability of age determination using this mass spectrometer is thus well-established.

Nagao et al. (1996) also lists a number of national standard samples (Zao basalt, JG-1, etc.) which are measured from time to time as internal standards. Among these, we measured Baba Tuff-2 several times to ascertain the accuracy of our Ar measurements (Table 3). The age we obtained (11.9 ± 0.1 Ma, two analyses) was quite consistent with the average of nine analyses done on the same sample at ISEI (11.8 ± 0.1 Ma) (Nagao et al., 1996).

The experimental results are summarized in Table 4. This table shows that our sample selection criteria worked remarkably well. There are six samples which did not meet the criteria, but are nevertheless used in K–Ar analysis (marked by a † in Table 4). The ages for two of them (TH11A-1 and TH11A-2) are quite reasonable, one (ES02) may have a larger error but is still usable, but the rest (ES04, ES03, BD02A) are definitely too old in comparison with the stratigraphic position (Fig. 2). In the latter three, in particular, the air contamination is quite high ($\approx$ 95%) and the quantity of ^{36}Ar is abnormally large.

For the samples where replicate analyses were done, reasonable agreement was obtained (TH11A, TH07 and BD04 in Table 4). Other ages also seem to be consistent with the stratigraphic position. Thus, we can conclude that the K–Ar ages obtained from the samples satisfying the foregoing criteria are quite reliable. Fig. 2 shows that these ages are in reason-

Table 3
Calibration of ages for modified VG5400 mass spectrometer at ISEI
K: Potassium content; *N*: number of independent analyses, or number of laboratories reporting data in case the number is preceded by > sign; $[^{40}Ar]_{rad}$: radiogenic ^{40}Ar in unit of 10^{-8} cm^3 STP/g; Age: in Ma. Standard data are from Flisch (1982) for Bern 4B and Bern 4M, Samson and Alexander (1987) for MMhb-1, and Jäeger et al. (1985) for BB-6. ISEI data from Nagao et al. (1996), except the last line (Baba Tuff-2, 2 analyses) which is from the present study. All the uncertainties are at 1σ level.

Sample	Standard data				Data from ISEI		
	K (wt.%)	*N*	$[^{40}Ar]_{rad}$ (10^{-8} cm^3 STP/g)	Age (Ma)	*N*	$[^{40}Ar]_{rad}$ (10^{-8} cm^3 STP/g)	Age (Ma)
Bern 4B (Biotite)	7.91	> 10	530 ± 11	17.2 ± 0.5	4	527.1 ± 0.8	17.09 ± 0.02
Bern 4M (Muscovite)	8.68	> 20	626 ± 17	18.5 ± 0.6	10	598 ± 34	17.8 ± 0.7
MMhb-1 (Hornblende)	1.555	> 18	3642 ± 11	520.4 ± 1.7	6	3658 ± 74	523 ± 9
BB-6 (Basalt)	1.68	16	2.88 ± 0.08	0.441 ± 0.013	3	3.01 ± 0.10	0.458 ± 0.016
Baba Tuff-2 (Biotite)	6.56				10	301.7 ± 2.5	11.81 ± 0.10
					2	303.5 ± 2.1	11.88 ± 0.08

Table 4
Results of K–Ar dating of Jökuldalur basalts
All the uncertainties are quoted at 1σ level. For samples with † see Section 4. Mean values (weighted by the inverse of individual variances) are given when replicate analyses are available. Ages are calculated with $\lambda_e = 0.581 \times 10^{-10}$ yr^{-1}, $\lambda_\beta = 4.962 \times 10^{-10}$ yr^{-1}, and $^{40}K/K = 1.167 \times 10^{-4}$ (Steiger and Jäger, 1977).

Sample	K (wt.%)	Ar sample weight (g)	^{36}Ar (10^{-10} cm^3 STP/g)	$^{40}Ar/^{36}Ar$	$[^{40}Ar]_{rad}$ (10^{-8} cm^3 STP/g)	Age (Ma)	$[^{40}Ar]_{rad}$ (%)
AD04	0.431	0.3396	4.04	328.2 ± 0.6	1.300 ± 0.026	0.78 ± 0.02	9.81
AD03	0.199	0.3327	1.69	345.6 ± 1.0	0.841 ± 0.021	1.09 ± 0.03	14.34
AD03A	0.270	0.3547	2.37	343.9 ± 0.8	1.140 ± 0.023	1.08 ± 0.02	13.94
AD02	0.264	0.3276	11.04	305.3 ± 0.5	1.030 ± 0.058	1.00 ± 0.06	3.04
AD01	0.314	0.3711	2.99	339.4 ± 0.6	1.300 ± 0.023	1.07 ± 0.02	12.79
TH15A	0.140	0.3434	2.41	308.7 ± 0.5	0.306 ± 0.014	0.56 ± 0.03	4.12
TH15	0.126	0.3119	2.97	303.9 ± 0.0	0.233 ± 0.013	0.48 ± 0.03	2.59
TH14	0.323	0.3603	1.98	353.3 ± 1.1	1.140 ± 0.025	0.91 ± 0.02	16.23
TH13	0.337	0.3250	5.99	316.6 ± 0.6	1.240 ± 0.035	0.95 ± 0.03	6.52
TH11A-1†	0.298	0.3173	5.61	321.2 ± 0.5	1.410 ± 0.029	1.22 ± 0.03	7.84
TH11A-2†	0.298	0.3153	7.31	314.2 ± 0.5	1.330 ± 0.035	1.15 ± 0.03	5.79
TH11A					(mean age)	1.18 ± 0.04	
TH11	0.268	0.3143	2.64	339.2 ± 0.8	1.140 ± 0.025	1.10 ± 0.03	12.73
TH10	0.228	0.3247	13.85	301.8 ± 0.3	0.806 ± 0.047	0.91 ± 0.05	1.93
TH09	0.227	0.3133	14.25	303.4 ± 0.4	1.050 ± 0.075	1.20 ± 0.09	2.43
TH08	0.251	0.3188	9.35	305.0 ± 0.5	0.997 ± 0.055	0.91 ± 0.06	2.94
TH07-1	0.320	0.3709	6.69	314.8 ± 0.5	1.260 ± 0.033	1.01 ± 0.03	5.97
TH07-2	0.320	0.3580	7.59	311.5 ± 0.4	1.180 ± 0.031	0.95 ± 0.03	4.98
TH07					(mean age)	0.98 ± 0.03	
TH06	0.428	0.3180	5.10	336.8 ± 0.5	2.090 ± 0.034	1.25 ± 0.02	12.12
TH05	0.377	0.3387	2.26	377.5 ± 1.2	1.850 ± 0.024	1.26 ± 0.02	21.70
TH04	0.154	0.3774	8.39	304.7 ± 0.4	0.728 ± 0.035	1.22 ± 0.06	2.59
TH02	0.164	0.2991	8.77	305.1 ± 0.5	0.801 ± 0.047	1.26 ± 0.07	2.99
ES05	0.252	0.3150	2.60	345.1 ± 0.9	1.280 ± 0.027	1.30 ± 0.03	14.22
ES04†	0.146	0.3156	34.26	300.3 ± 0.4	1.480 ± 0.119	2.61 ± 0.21	1.44
ES03†	0.186	0.3039	29.47	302.1 ± 0.4	1.790 ± 0.112	2.47 ± 0.16	2.00
ES02†	0.172	0.3280	6.67	310.7 ± 0.4	0.980 ± 0.030	1.47 ± 0.05	4.74
ES01	0.277	0.3108	6.14	327.8 ± 0.5	1.950 ± 0.035	1.82 ± 0.04	9.69
BD05	0.193	0.3396	12.82	303.8 ± 0.4	1.000 ± 0.047	1.33 ± 0.06	2.56
BD04-1	0.187	0.3119	2.20	343.6 ± 0.9	1.050 ± 0.024	1.44 ± 0.04	13.86
BD04-2	0.187	0.3152	2.53	348.8 ± 0.7	0.990 ± 0.019	1.36 ± 0.03	11.58
BD04					(mean age)	1.40 ± 0.04	
BD03	0.413	0.3529	2.41	392.9 ± 1.3	2.340 ± 0.030	1.46 ± 0.02	24.69
BD02A†	0.190	0.3070	56.59	300.5 ± 0.4	2.540 ± 0.202	3.43 ± 0.28	1.49
KG02	0.214	0.3219	3.98	325.2 ± 0.5	1.160 ± 0.023	1.40 ± 0.03	8.97
KG01	0.203	0.3173	3.08	337.5 ± 0.7	1.280 ± 0.024	1.62 ± 0.03	12.29
KG00	0.205	0.3238	14.81	304.7 ± 0.4	1.290 ± 0.057	1.61 ± 0.07	2.85
KG00A	0.286	0.3149	3.55	354.0 ± 0.8	2.060 ± 0.034	1.85 ± 0.04	16.39

ably good agreement with the stratigraphic position of the lava flows.

5. Interpretation of magnetostratigraphy

Watkins et al. (1975) reported paleomagnetic results from GK (our KG) as well as three other sections (GH, GJ, and GL), which are about 10 km NNE from the GK section and along Hnjuksá (GH), Tregagilsá (GJ), and Arnorsstadahnjukur (GL) streams. K–Ar ages were obtained from lavas of GH and GL sections, which contained the stratigraphic units 16 and 17 of Wensink (1964a,b) corresponding to the Gilsá event. The ages they obtained for the

Table 5
Comparison of mean ChRM directions in the KG section
The number of samples are four in (Watkins et al., 1975) and five in this study. Age data are from this study only.

Watkins et al. (1975)				Present study				
Lava	I (°)	D (°)	α_{95} (°)	Lava	I (°)	D (°)	α_{95} (Ma)	Age
GK9	−55.3	155.7	6.6	KG02	−59.4	154.4	4.2	1.40 ± 0.03
GK4	83.8	39.8	4.2	KG01	81.8	8.6	2.5	1.62 ± 0.03
GK2	69.9	36.1	3.0	KG00	66.7	29.5	2.6	1.61 ± 0.07
				KG00A	−61.2	167.4	5.7	1.85 ± 0.04

normal flows in GH and GL sections were 1.53, 1.55, 1.68, 1.63, and 1.57 Ma, in good agreement with the earlier work of McDougall and Wensink (1966). As for the GJ and GK sections, their correlation was based on the stratigraphic descriptions of Wensink (1964b) and they did not carry out dating of lava flows there. Our paleomagnetic results from KG samples are in very good agreement with those of Watkins et al. (1975). Table 5 compares the magnetization directions in Watkins et al. (1975) and the present study. The ChRM directions of KG00, KG01, and KG02 are in reasonable agreement with those reported for GK2, GK4, and GK9 (Table 5).

Wensink (1964b) found it quite difficult to correlate the lava flows in the southern part of Jökuldalur owing to the presence of tectonic complications such as faults. Thus, his correlation south of and including the KG is not very clear (see his Fig. 9). Fig. 2 of Wensink (1964b) shows that the normal flows in R_1 series extends to KG and BD, but that was omitted from his summary stratigraphic column (Fig. 9). In the KG and BD sections, Wensink (1964b) suggested a N–S trending fault just at the magnetic N–R boundary, implying that the reversed polarity found at lower parts may be a repetition of the ones at higher levels. However, we did not find any evidence of such faults in the field. The K–Ar ages from KG and BD sections as well as our field observation suggests that there is no significant gap or duplication in these sections.

Watkins et al. (1975) thought that the lower reversed lavas in the GK section correspond to Gauss chron (N_2), and denied the existence of Gilsá age flows as suggested by Wensink (1964b) (Fig. 2). However, we find that this correlation is wrong. Good Gilsá ages were obtained for the normal lavas KG00 and KG01. There is a reversed flow (KG00A) below this normal which was previously not sampled. The K–Ar age obtained for this flow (1.85 ± 0.04 Ma) falls in the Olduvai normal subchron (1.77 to 1.95 Ma, according to Cande and Kent, 1995). Apparently, the K–Ar age for KG00A is either too young or too old, since self-reversal for this flow is highly unlikely (see Appendix A). It should be stressed that KG00A is distinctly younger than the Gilsá event in any case. If this K–Ar age is too old, KG00A belongs to a short reversed period between Olduvai and Gilsá.

From these considerations, it seems reasonable to conclude that we have the normal lavas in both KG and BD sections which corresponds to the Gilsá subchron discovered originally in the northern part of Jökuldalur. From these results, the zone of lava flows representing the Gilsá normal event extends from the GH section where it was originally discovered to the KG and BD sections which are about 10 km to the southwest (Fig. 1).

We obtained an age of 1.82 ± 0.04 Ma for the normally magnetized ES01, which makes this flow a candidate for the Olduvai age. The stratigraphic correlation is not inconsistent with this interpretation. But we cannot be too sure of this possibility, since this is a result obtained from a single flow and not in succession. Another point to be noted is that the

Fig. 7. The VGP latitudes, magnetic polarity inferred from our study, and K–Ar ages for the composite section in the Jökuldalur area compared with the standard polarity time scale of Cande and Kent (1995). The height of each section was adjusted as described in the text. Note the good linear trend between the height and K–Ar age. The topmost two normal data are from TH15 and TH15A which are separated from lower flows by conglomerate. The bottom normal lava (ES05) can be about 100 m higher, considering its position relative to the TH section (see text).

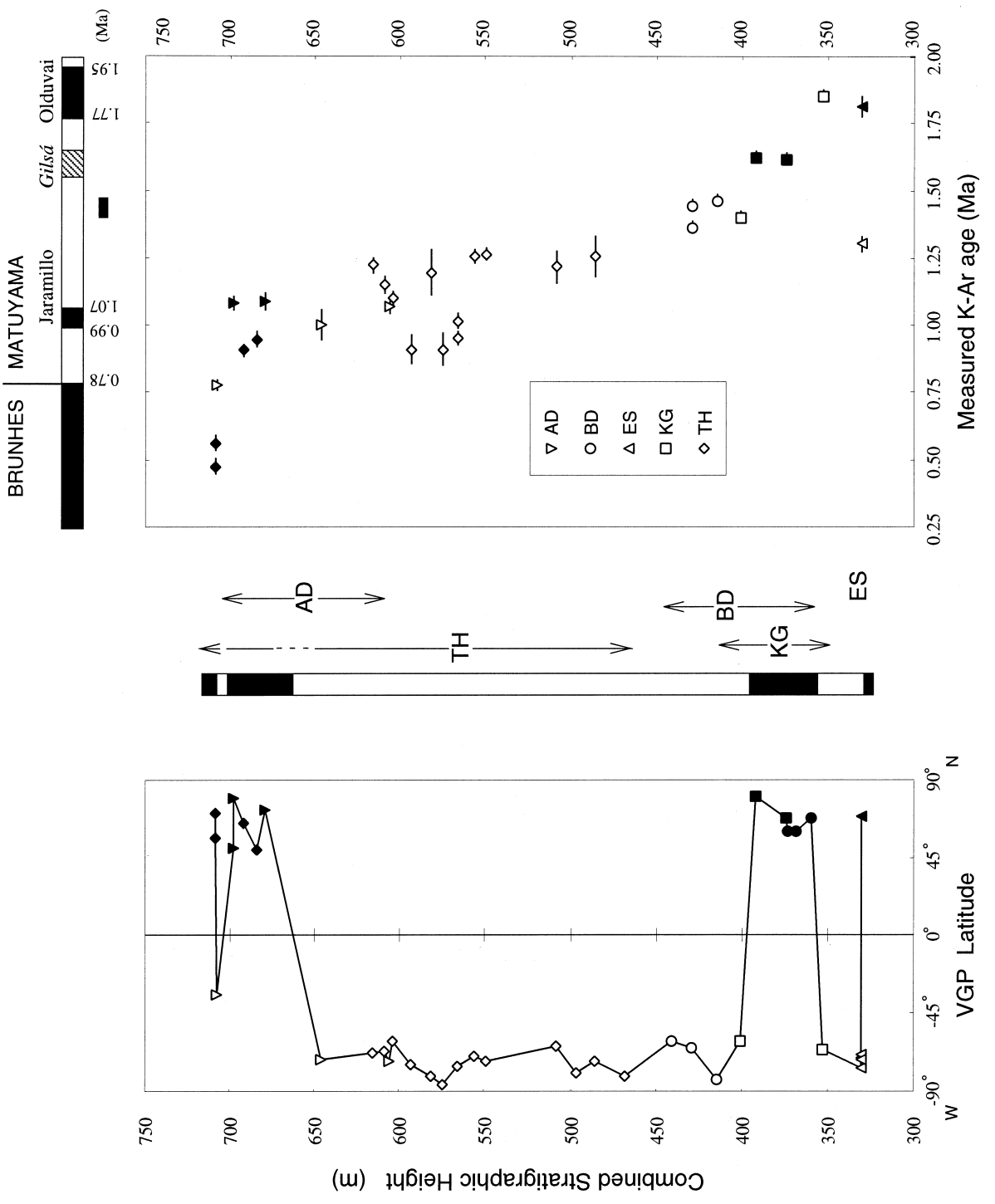
BRUNHES
MATUYAMA
Jaramillo
Gilsá
Olduvai
(Ma)
1.95
1.77
1.07
0.99
0.78
AD
BD
ES
KG
TH
Measured K-Ar age (Ma)
Combined Stratigraphic Height (m)
VGP Latitude
W
N
-90°
-45°
0°
45°
90°

ChRM direction of ES01 ($I = 66.3°$, $D = 25.5°$) is rather close to that of KG00 ($I = 66.7°$, $D = 29.5°$), which we identified as Gilsá normal. Although the uncertainties in the K–Ar ages in the present study seem to be less than about 0.1 Ma, we cannot eliminate the possibility that this particular age has a much larger error and ES01 lava is identical to KG00, and thus of Gilsá age.

In the southwestern part of the present study area, the R–N–R sequence in the AD section can be correlated to Matuyama–Jaramillo–Matuyama just below the Brunhes–Matuyama boundary. On the other hand, most of the TH section (TH01 to TH12) belong to Matuyama reversed, but the topmost four layers corresponds to Jaramillo (TH13 and TH14) and Brunhes normal (TH15 and TH15A). The existence of a conglomerate layer between TH14 and TH15 is in excellent agreement with the large age gap observed between the K–Ar ages of lower and upper flows. Thus, in all, the sections we studied in the Jökuldalur covers the period from just above the Olduvai through upper Matuyama, Jaramillo normal, the reversed period just below Brunhes–Matuyama boundary, and to the middle of Brunhes normal. ES01 lava may correspond to the Olduvai normal, but there is also a possibility that its K–Ar age is about 0.2 Ma too old and it actually belongs to Gilsá.

The composite stratigraphic section of Jökuldalur was made from the data of five sections and shown in Fig. 7. In constructing the composite section, simplest match was sought which is consistent with the general dip of strata in Jökuldalur as well as the magnetic polarities observed. TH and BD sections, respectively, were placed 100 and 30 m higher than the actual elevation shown in Table 1, which is not in conflict with the observed regional dip of 1 to 2° to the west. Other sections (GK, ES, AD) were placed at their observed heights. In all cases, the relative height in each section was unchanged. The position of the AD section is not consistent with the regional dip, but offset may be caused by unknown fault as we did not examine the Hrafnkelsdalur as closely as we did between KG and TH in Jökuldalur.

Fig. 7 shows that this quite simple adjustment can produce a very good single composite section. In fact, if we exclude the data from ES05, of which the stratigraphic position is not certain, and TH15 and TH15A, which are separated from the lower flows by a considerable time gap as represented by a conglomerate layer, all the data define a broadly linear relation between the stratigraphic height and age. Moreover, they show that assignment of these data to the upper part of Matuyama (from Olduvai through Gilsá and Jaramillo to lower Brunhes) is quite reasonable, judging from the magnetic polarities of the flows.

Among the ages in Fig. 7, those for TH07, TH08, and TH10 may be too young by 0.1 to 0.2 Ma. This amount is too large compared to the experimental errors of 0.03 to 0.06 Ma as quoted in Table 4. The 1σ errors of Table 4 give only the experimental uncertainty, and their values are quite reasonable as can be seen by the fact that replicate analyses gave the standard deviations which are quite similar to these values. The small 1σ error, as well as the reproducibility of the K–Ar ages from multiple samples from the same flow, indicate the good experimental condition for the ISEI mass spectrometry system. This does not, however, exclude the possibility of obtaining the stratigraphically inconsistent data as shown by the ages of TH07, TH08 and TH10. Uncertainties in ages are not restricted to the experimental ones, but can arise from loss or gain of Ar or K caused by geological situations and which will not affect the experimental results (including the errors).

Udagawa (1997) made the major element analysis of all these lava samples by X-ray diffraction method. These data show that phosphor, which behaves similarly to K, does not show depletion in these samples. Thus, we can deny the possibility of K loss. Existence of excess Ar may be a possibility in some of the samples. As often observed in dating analyses, we must admit that the *true* or geological uncertainty in the ages obtained in this study is about 0.1 Ma.

6. Discussion

There is no ambiguity in the determination of ChRM directions for the samples in this study. In most cases, the results of AF demagnetizations were very simple and the primary magnetization could be obtained by a straightforward application of the principal component analysis (Kirschvink, 1980). Consideration about the remagnetization circle was necessary only in two flows, but excellent convergence

was observed even in these two flows (TH13 and TH14) when the combined analysis of McFadden and McElhinny (1988) was applied to the great circles and fixed points (Fig. 5). In all flow units, the mean directions of magnetization could be determined with very small confidence angles (Table 1). Thus, the present paleomagnetic results are quite reliable.

The K–Ar ages for the Jökuldalur lavas are also very well-determined. Although the K content is rather low in these tholeiitic basalts, use of adequate sample selection criteria and a high resolution mass spectrometer (Nagao et al., 1996) made it possible to obtain reliable ages with very small experimental errors (see Table 4 and Fig. 2). Our data from the KG section show that this continuous section has R–N–R magnetic polarities and K–Ar ages of all the normal lavas are younger than Olduvai. Results from the BD section are not so conclusive, but are consistent with this interpretation. Thus, there is very small possibility that the age of Gilsá lavas can be increased to fit into the Olduvai subchron. Together with the paleomagnetic data, these high quality age data suggest that the Gilsá event is a short normal interval different from the well-documented Olduvai subchron.

As discussed earlier, the Gilsá event is not included in the more recent standard geomagnetic polarity time scales (GPTS). This may be attributable to the fact that the GPTS is constructed mainly from marine magnetic anomaly data (e.g., Cande and Kent, 1992, 1995). Because of the separation of the source (magnetized layer in the bottom of the sea) and observation level (sea surface), marine magnetic anomalies cannot deal with very short polarity episodes which may be recorded in width much shorter than the depth of the ocean. To look for the evidence of short events such as Gilsá, we have to turn to data from sediments or lava flows which deposited rapidly in the particular period.

Clement and Kent (1987) made a detailed study of Deep Sea Drilling Project (DSDP) Site 609 cores (49.86°N, 24.23°W), and found that Gilsá event lasted about 4600 years with a mean age of 1.55 Ma. They concluded that Gilsá was not a true reversal but a magnetic excursion, because magnetization directions did not exhibit a sustained interval of normal polarity.

Tauxe et al. (1983) found a short normal period above Olduvai normal in the sediments from the Vrica section, southern Italy, which is the stratotype section of the Plio–Pleistocene boundary. A later study by Zijderveld et al. (1991) denied the existence of thin reversed part between two normal sequences in the Vrica section reported by Tauxe et al. (1983). However, these authors found an additional zone of normal polarity about 4 m above, and a similar N–R–N sequence at the corresponding heights in the nearby Crotone section. Zijderveld et al. (1991) discussed the two possibilities of interpreting this sequence: they are (1) Olduvai subchron contain a short reversed polarity at the top part, or (2) a separate normal subchron (''Vrica subchron'') exists just after the Olduvai. They did not identify this normal period with Gilsá, because of the ambiguity in the original definition of Gilsá event (McDougall and Wensink, 1966; Watkins et al., 1975), and also because they thought that Gilsá belongs to isotopic stage 54 and the Vrica to stage 64. The astronomically calibrated time scale of Hilgen (1991) was constructed using these data. Interestingly, Zijderveld et al. (1991) placed the sapropel zones q to s of Vrica section, where Tauxe et al. (1983) found normal polarity and identified with Jaramillo subchron, to about 1.5 to 1.6 Ma, but they did not find normal polarity there.

Similar short polarity transitions were also reported from the loess of China. Heller et al. (1991) reported a short normal period above the Olduvai subchron from the loess section of Xifeng (35.5°N, 107.5°E). More recently, Li et al. (1997) reported the results of detailed magnetostratigraphic study of the loess in Linxia Basin (35.5°N, 108°E) and found a short normal zone at about 1.53 Ma which they identified as the ''stage 54'' event (Zijderveld et al., 1991).

The interpretation of the above results are not unanimous about the existence or absence of Gilsá event. The results from the Vrica section is especially complicated. However, we may infer the existence of a short normal period at about 1.5–1.6 Ma, distinct from the more established Olduvai. This conclusion is supported by sediment data from North Atlantic (Clement and Kent, 1987; Channell and Lehman, 1997b) as well as from Chinese loess (Li et al., 1997).

Some more new findings came from the recent Ocean Drilling Program (ODP) results. One is from Leg 162, which took cores from a number of sites in the North Atlantic near Iceland (Channell and Lehman, 1997a). A short normal episode on top of the Olduvai normal was recorded in multiple cores from this leg indicating the presence of ''Gilsá'' or ''stage 54'' events (Channell and Lehman, 1997b). Another report is from the Baja California area drilled in Leg 167 of ODP. Hayashida et al. (1998) also found a distinct but very short normal period just above the extensive Olduvai. Together with the identification of the intensity minimum around 1.67 Ma found in cores drilled in the equatorial Pacific in Leg 138 (Valet and Meynadier, 1993), these ODP results indicate that Gilsá is a short normal just above the well-established Olduvai subchron. Our data from Jökuldalur in Eastern Iceland give strong support to this conclusion.

7. Conclusions

We have carried out a paleomagnetic and K–Ar dating study of five basaltic lava sections in Jökuldalur, Eastern Iceland. One section was the same as the GK section studied by Watkins et al. (1975). We obtained very high quality results both in paleomagnetism and K–Ar analysis. The magnetic polarities and K–Ar ages indicate that these lavas cover the Matuyama–Brunhes period mainly for the interval of 1.8–0.8 Ma, but continues to about 0.5 Ma with a small age gap.

A few lava flows show normal polarity with an age of about 1.6 Ma, in agreement with the Gilsá event studied by McDougall and Wensink (1966) and Watkins et al. (1975). There is a reversed lava below the Gilsá lavas, which gave an age in the Olduvai normal. We may assign this lava to the normal period just above the well-established Olduvai subchron, but there is also a possibility that this lava is younger than Olduvai. Thus, the existence of Olduvai age lavas below Gilsá was inferred but not confirmed. The magnetic polarity changes inferred from the composite section (Fig. 7) are quite consistent with the standard time scale of geomagnetic polarity changes (Cande and Kent, 1995), but need that the Gilsá normal event be included.

The existence of short normal event (Gilsá) just above but distinct from Olduvai seems to be supported by newer data from marine as well as from continental sediments.

The distribution of VGPs calculated from the present set of data does not show significant departure from the geographic pole. The far-sidedness or right-handedness of the poles often inferred as the general feature of the Plio–Pleistocene paleomagnetic field cannot be supported by the present data.

Acknowledgements

We are grateful to Keisuke Nagao and Ichiro Kaneoka for the use of their mass spectrometer and flame photometer. We thank Akio Makishima and Ken'ichi Kawamura for logistic support in the field works. Keisuke Nagao and Yayoi Miura kindly offered suggestions for improvements of the manuscript. Comments by two anonymous reviewers were quite helpful in revising the paper. The sampling was carried out with a grant-in-aid from Monbusho (05041059). The spinner magnetometer–AF demagnetizer system used in paleomagnetic measurements was developed and constructed with another Monbusho grant (06452075).

Appendix A. Rock magnetic properties

One reviewer commented that mineralogical analysis of the magnetic minerals is necessary for this study. We have carried out an extensive series of experiments as requested. The results are summarized below.

All the rock magnetic experiments were carried out using Princeton model 2900 vibration sample magnetometer. At least one sample from each flow was subjected to hysteresis measurements (for determination of saturation magnetization J_s, saturation remanence J_r, and coercivity H_c), DC magnetization (for acquisition of isothermal remanent magnetization IRM), DC demagnetization of saturation IRM (for remanence coercivity H_{cr}), and thermomagnetic analysis (for Curie temperature T_c). Slope corrections were applied in the calculation of J_s from hysteresis data to account for the existence of paramagnetic

component. Saturation IRM was induced in a field of about 0.5 T. Temperatures in thermomagnetic measurements were calibrated by measurements of nickel and magnetite. Table 6 summarizes the hysteresis parameters and Curie temperature of the Jökuldalur lavas.

Fig. 8 shows the results of experiments for two lavas in the TH section, which are typical examples of low- and high-T_c magnetic carriers in the present samples. The first group has Curie temperatures around 200°C suggesting that the magnetic minerals are nearly unoxidized titanomagnetite, while the T_cs

Table 6
Summary of rock magnetic properties of Jökuldalur lavas
N_T, N_H, N_D: number of samples for thermomagnetic (T_c), hysteresis (J_s, J_r, H_c), and demagnetization (H_{cr}) measurements; T_c: Curie temperature; J_s: saturation magnetization; J_r: saturation remanence; H_c: coercivity; H_{cr}: remanence coercivity; σ: standard deviation (%), given only when multiple data are available from the same lava flow.

Flow	Sample			T_c		J_s		J_r		H_c		H_{cr}		J_r/J_s		H_c/H_{cr}	
	N_T	N_H	N_D	Mean (°C)	σ (%)	Mean (A m^2/kg)	σ (%)	Mean (A m^2/kg)	σ (%)	Mean (mT)	σ (%)	Mean (mT)	σ (%)	Mean	σ (%)	Mean	σ (%)
AD04	1	1	1	184		0.863		0.307		7.9		13.8		0.356		1.749	
AD03	1	2	1	242		0.657	41	0.192	40	8.0	1	15.9		0.293	1	1.963	
AD03B	1	2	1	509		0.569	7	0.169	3	11.5	11	24.4		0.298	3	2.313	
AD03A	1	1	1	336		0.387		0.102		7.4		13.1		0.264		1.765	
AD02	1	3	1	585		0.629	24	0.202	32	13.3	16	26.4		0.317	11	2.064	
AD01	1	1	1	336		0.554		0.128		3.7		7.5		0.230		2.015	
TH15A	1	1	1	381		0.420		0.127		6.5		12.6		0.301		1.944	
TH15	1	1	1	221		0.285		0.073		3.6		8.1		0.256		2.233	
TH14	1	2	2	184		0.266	7	0.140	7	7.9	10	13.2	14	0.528	0	1.667	4
TH13	4	10	6	190	4	0.225	10	0.119	13	8.8	9	15.5	11	0.525	4	1.639	4
TH12	1	2	1	580		1.335	10	0.293	1	15.4	0	29.4		0.220	8	1.915	
TH11A	1	3	1	536		2.586	25	1.103	25	28.4	6	46.7		0.427	6	1.565	
TH11	2	6	1	526	0	0.956	12	0.201	8	6.0	2	12.5		0.211	6	2.073	
TH10	2	5	1	590	0	0.602	7	0.178	6	16.4	1	33.3		0.296	2	2.054	
TH09	1	2	1	587		0.685	9	0.178	7	14.1	3	29.9		0.260	1	2.066	
TH08	1	2	1	581		0.725	13	0.169	7	13.6	0	27.8		0.234	6	2.036	
TH07	1	1	1	330		0.682		0.204		7.6		13.5		0.300		1.776	
TH06	1	3	1	583		0.946	5	0.223	6	8.4	13	13.7		0.236	4	1.914	
TH05	2	7	1	568	0	0.799	39	0.187	38	6.9	5	12.7		0.235	4	1.978	
TH04	1	1	1	222		0.585		0.165		9.3		20.2		0.282		2.164	
TH03	1	1	1	225		0.220		0.054		3.5		8.1		0.247		2.322	
TH02	1	1	1	310		0.256		0.065		5.8		11.9		0.254		2.070	
TH01	1	2	1	235		0.505	13	0.105	1	3.6	1	7.1		0.209	11	2.002	
ES05	1	3	2	224		0.726	15	0.130	16	4.1	1	7.4	3	0.179	0	1.795	0
ES04	1	1	1	254		0.401		0.109		4.6		7.7		0.272		1.669	
ES03	1	2	1	581		0.696	16	0.181	7	15.4	13	32.7		0.262	9	1.948	
ES02	1	1	1	227		0.288		0.090		6.6		10.7		0.312		1.627	
ES01	1	2	1	498		1.779	5	0.249	6	8.1	5	18.6		0.140	11	2.382	
BD05	1	3	1	605		1.022	1	0.337	2	21.5	1	41.6		0.329	3	1.964	
BD04	1	1	1	189		0.361		0.058		2.8		5.3		0.159		1.903	
BD03	1	1	1	196		0.450		0.191		9.8		17.4		0.424		1.775	
BD02A	1	2	1	570		1.062	0	0.242	8	10.2	1	19.1		0.228	9	1.900	
BD02	1	2	1	570		0.632	1	0.182	4	12.2	0	25.2		0.289	6	2.061	
BD01	1	3	1	603		1.477	13	0.498	10	29.0	1	47.2		0.338	4	1.653	
GK02	1	2	1	586		1.219	0	0.356	5	16.2	6	31.0		0.292	4	1.995	
GK01	2	6	1	584	0	0.903	3	0.244	4	14.9	0	29.6		0.271	1	1.989	
GK00	1	2	1	588		0.998	21	0.185	0	12.3	2	26.4		0.190	20	2.187	
GK00A	1	4	1	233		0.874	7	0.510	11	17.0	4	23.0		0.582	4	1.389	

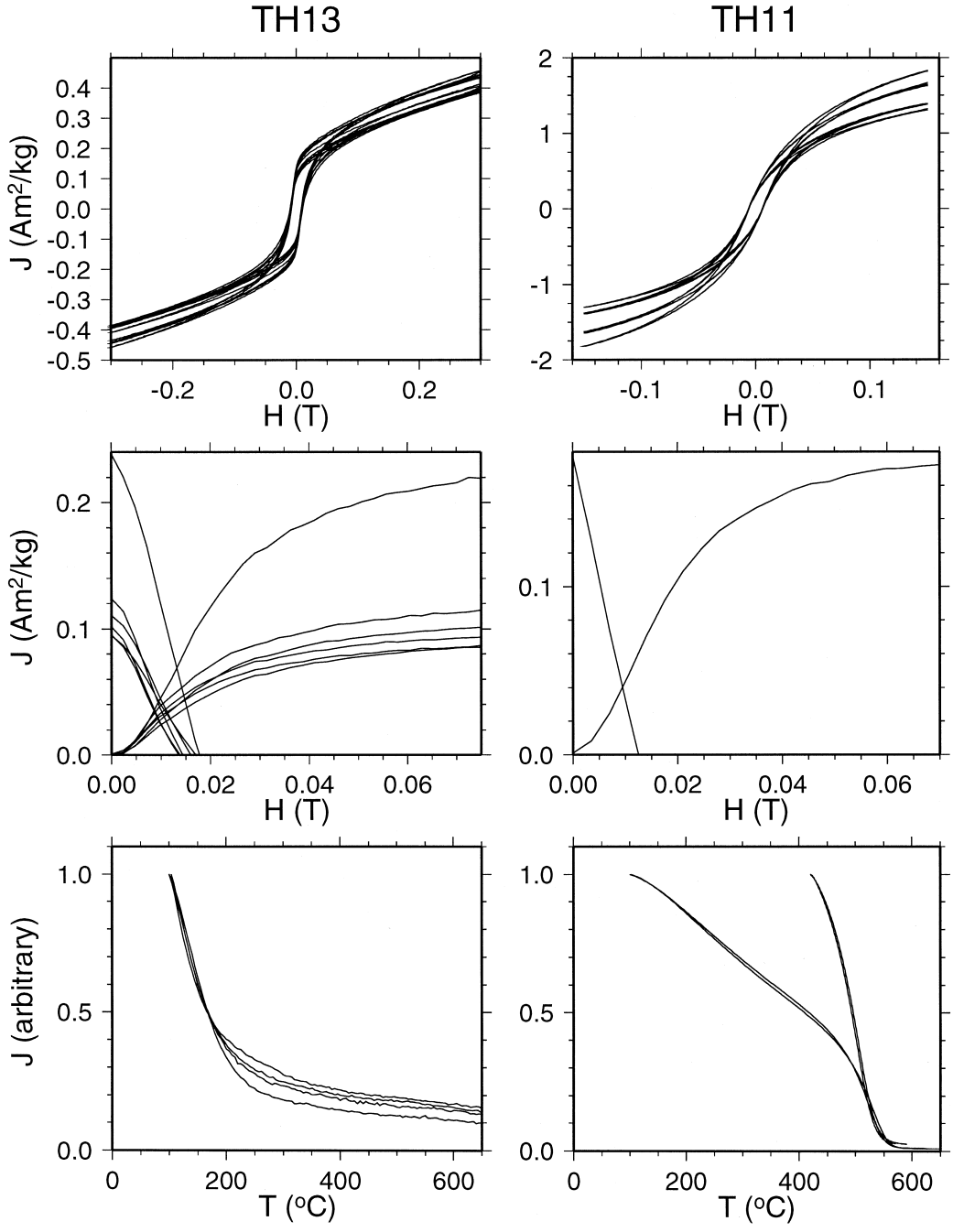

Fig. 8. Examples of hysteresis measurements (top), DC magnetization and demagnetization (middle), and thermomagnetic experiments (bottom). TH13 and TH11 are representative of low- and high-T_c samples, respectively. Only heating curves are shown for thermomagnetic analysis.

of the second group concentrate close to that of magnetite (585°C). Such combination is quite reasonable for subaerial basalts which underwent various degrees of high-temperature oxidation (Larson et

al., 1969). The fact that the magnetic carriers in these basalts are titanomagnetites or magnetites is further supported by the response to DC field: saturation IRM can be attained in a field of about 50 mT, and demagnetitized at smaller fields. The median destructive field in AF demagnetization in most samples is 10–20 mT (Figs. 3–5), in agreement with the H_{cr} values.

Fig. 9 shows the correlation between hysteresis parameters and Curie temperature. The histogram of

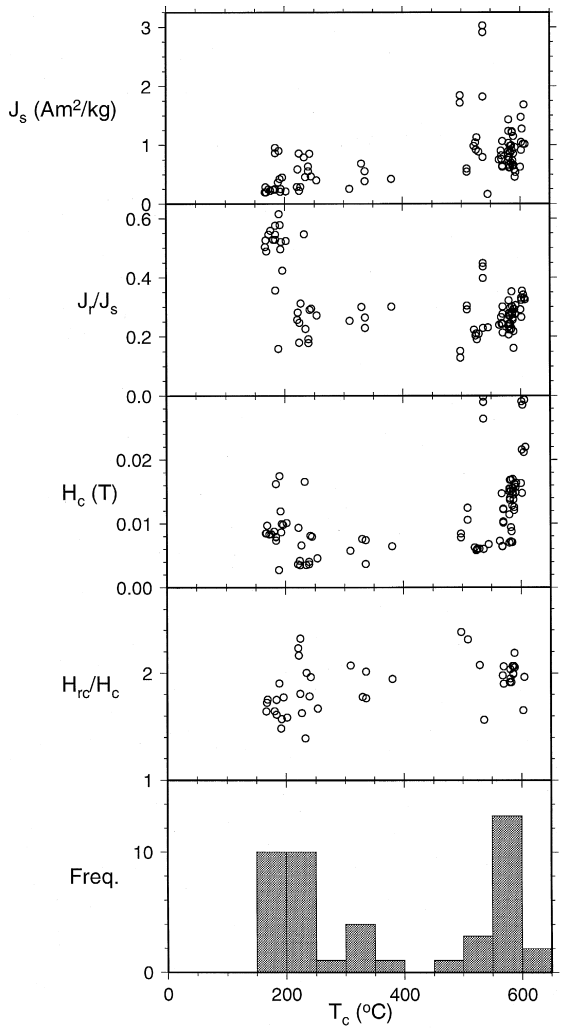

Fig. 9. Correlation of various hysteresis parameters with the Curie temperature. Circles correspond to individual samples (not lava means). The bottom panel shows the number of samples with T_c in each 50°C intervals.

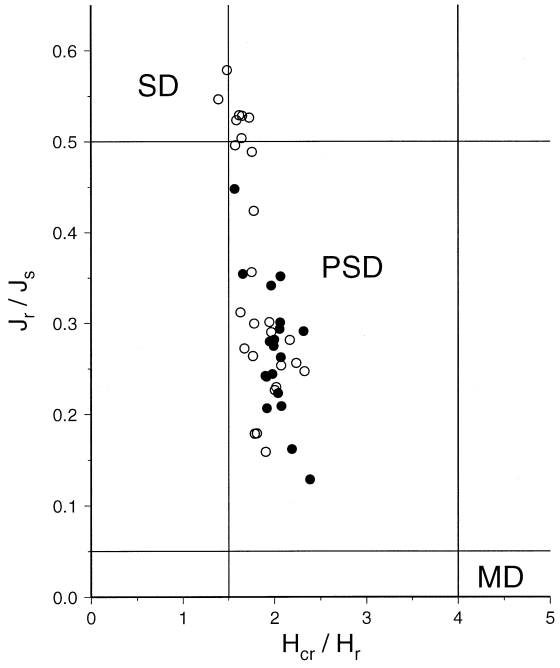

Fig. 10. Day diagram for the present samples (Day et al., 1977). Open and filled symbols indicate samples of low- and high-T_c groups, respectively.

T_c is remarkably bimodal. The very high H_c values for some of the high-T_c samples may be caused by the subdivision of grains in high-temperature oxidation (Larson et al., 1969).

Fig. 10 is the Day diagram showing the state of grains of these titanomagnetites and magnetites (Day et al., 1977). A small fraction of samples fall in the SD part, but most samples are in the PSD region closer to SD than to the multidomain (MD) part.

All the results of rock magnetic experiments show that the carriers of the remanence in Jökuldalur basalts are originally titanomagnetites which underwent various degrees of subaerial high-temperature oxidation. It is quite well-known that the NRM in such rocks can be quite good recorders of the past magnetic field.

References

Ando, A., Mita, N., Matsumoto, A., 1989. 1987 compilation of K_2O concentrations in seventeen GSJ rock reference samples, igneous rock series. Bull. Geol. Surv. Jpn. 40, 19–45.

Cande, S.C., Kent, D.V., 1992. A new geomagnetic polarity timescale for the Late Cretaceous and Cenozoic. J. Geophys. Res. 97, 13917–13951.

Cande, S.C., Kent, D.V., 1995. Revised calibration of the geomagnetic polarity timescale for the Late Cretaceous and Cenozoic. J. Geophys. Res. 100, 6093–6095.

Channell, J.E.T., Lehman, B., 1997a. The last two geomagnetic polarity reversal recorded in high-deposition-rate sediment drifts. Nature 389, 712–715.

Channell, J.E.T., Lehman, B., 1997b. Magnetic events, secular variation and paleointensity at ODP sites 983 and 984 (North Atlantic). Abstracts, IAGA Uppsala Assembly, p. 43.

Clement, B.M., Kent, D.V., 1987. Short polarity intervals within the Matuyama: transitional field records from hydraulic piston cored sediments from the North Atlantic. Earth Planet. Sci. Lett. 81, 253–264.

Cox, A., 1969a. Geomagnetic reversals. Science 163, 237–245.

Cox, A., 1969b. Confidence limits for the precision parameter K. Geophys. J. R. Astron. Soc. 18, 545–549.

Cox, A., Doell, R.R., Dalrymple, G.B., 1968. Radiometric timescale for geomagnetic reversals. Q. J. Geol. Soc. London 124, 53–66.

Day, R., Fuller, M.D., Schmidt, V.A., 1977. Hysteresis properties of titanomagnetites: grain size and composition dependence. Phys. Earth Planet. Inter. 13, 260–267.

Einarsson, T., 1973. Magnetic polarity groups in the Fljótsdalsheidi area, including Gilsá. Jökull 23, 53–58.

Fisher, R., 1953. Dispersion on a sphere. Proc. R. Soc. London, Ser. A 217, 295–305.

Flisch, M., 1982. Potassium–argon analysis. In: Odin, G.S. (Ed.), Numerical Dating in Stratigraphy. Wiley, Chichester, pp. 151–158.

Grommé, C.S., Hay, R.L., 1963. Magnetization of basalt of bed I, Olduvai Gorge, Tanganyika. Nature 200, 560–561.

Grommé, C.S., Hay, R.L., 1967. Geomagnetic polarity epochs: new data from Olduvai Gorge, Tanganyika. Earth Planet. Sci. Lett. 2, 111–115.

Grommé, C.S., Hay, R.L., 1971. Geomagnetic polarity epochs: age and duration of the Olduvai normal polarity event. Earth Planet. Sci. Lett. 10, 79–185.

Hayashida, A., Verosub, K.L., Heider, F., Leonhardt, R., 1998. Magnetostratigraphy and relative paleointensity data from pelagic sediments off Baja California (ODP Leg 167 Site 1010). Abstracts of 104th SGEPSS Fall Meeting, B22-P106, Mito, November 1998.

Heller, F., Liu, X., Liu, T., Xu, T., 1991. Magnetic susceptibility of loess in China. Earth Planet. Sci. Lett. 103, 301–310.

Hilgen, F.J., 1991. Astronomical calibration of Gauss to Matuyama sapropels in the Mediterranean and implication for the geomagnetic polarity time scale. Earth Planet. Sci. Lett. 104, 226–244.

Jäeger, E., Chen, W.J., Li, D.M., Liu, R.X., Hunziker, J.C., Hurford, A.J., 1985. BB-6 — a Quaternary age standard for K–Ar dating. Chem. Geol. 52, 275–279.

Kirschvink, J.L., 1980. The least-squares line and plane and the analysis of paleomagnetic data. Geophys. J. R. Astron. Soc. 62, 699–718.

Kono, M., Hamano, Y., Nishitani, T., Tosha, T., 1984. A new spinner magnetometer: principles and techniques. Geophys. J. R. Astron. Soc. 67, 217–227.

Kono, M., Kitagawa, H., Tanaka, H., 1997. Use of automatic spinner magnetometer–AF demagnetizer system for magnetostratigraphy and paleosecular variation studies. Abstracts, IAGA Uppsala Assembly, p. 66.

Kristjansson, L., Johannesson, H., 1989. Variable dispersion of Neogene geomagnetic field directions in Iceland. Phys. Earth Planet. Inter. 56, 124–132.

Larson, E.E., Ozima, M., Ozima, M., Nagata, T., Strangway, D., 1969. Stability of remanent magnetization of igneous rocks. Geophys. J. R. Astron. Soc. 17, 263–292.

Li, J.J., Fang, X.M., Van der Voo, R., Zhu, J.J., MacNiocaill, C., Ono, Y., Pan, B.T., Zhong, W., Wang, J.L., Sasaki, T., Zhang, Y.T., Cao, J.X., Kang, S.C., Wang, J.M., 1997. Magnetostratigraphic dating of river terraces: rapid and intermediate incision by the Yellow River of the northeastern margin of the Tibetan Plateau during the Quaternary. J. Geophys. Res. 102, 10121–10132.

McDougall, I., 1979. The present status of the geomagnetic polarity time scale. In: McElhinny, M.W. (Ed.), Earth: Its Origin, Structure and Evolution. Academic Press, London, pp. 543–566.

McDougall, I., Wensink, H., 1966. Paleomagnetism and geochronology of the Pliocene–Pleistocene lavas in Iceland. Earth Planet. Sci. Lett. 1, 232–236.

McFadden, P.L., McElhinny, M.W., 1988. The combined analysis of remagnetization circles and direct observations in palaeomagnetism. Earth Planet. Sci. Lett. 87, 161–172.

Merrill, R.T., McElhinny, M.W., 1977. Anomalies in the time-averaged paleomagnetic field and their implications for the lower mantle. Rev. Geophys. Space Phys. 15, 309–323.

Nagao, K., Ogata, A., Miura, Y.N., Yamaguchi, K., 1996. Ar isotope analysis for K–Ar dating using two modified-VG5400 mass spectrometers: 1. Isotope dilution method. J. Mass Spectrom. Soc. Jpn. 44, 39–61.

Nier, A.O., 1950. A redetermination of the relative abundances of the isotopes of carbon, nitrogen, oxygen, argon and potassium. Phys. Rev. 77, 789–793.

Ozima, M., Podosek, F.A., 1983. Noble Gas Geochemistry. Cambridge Univ. Press, London, 367 pp.

Samson, S.D., Alexander, E.C. Jr., 1987. Calibration of the interlaboratory ^{40}Ar–^{39}Ar dating standard. Chem. Geol. 66, 27–34.

Steiger, R., Jäger, E., 1977. Convention on the use of decay constants in geo- and cosmo-chronology. Earth Planet. Sci. Lett. 36, 359–362.

Tauxe, L., Opdyke, N.D., Pasini, G., Elmi, C., 1983. Age of the Plio–Pleistocene boundary in the Vrica section, southern Italy. Nature 304, 125–129.

Terashima, S., Imai, N., Itoh, S., Ando, A., Mita, N., 1994. 1993 compilation of analytical data for major elements in seventeen GSJ geochemical reference samples, igneous rock series. Bull. Geol. Surv. Jpn. 45, 305–381.

Udagawa, S., 1997. Geochemistry and Geochronology of Successive Lava Flows in Eastern Iceland. MSc Thesis, University of Tokyo, 97 pp., in Japanese.

Valet, J.-P., Meynadier, L., 1993. Geomagnetic field intensity and reversals during the past four million years. Nature 366, 234–238.

Watkins, N.D., Kristjansson, L., McDougall, I., 1975. A detailed paleomagnetic survey of the type location for the Gilsá geomagnetic polarity event. Earth Planet. Sci. Lett. 27, 436–444.

Wensink, H., 1964a. Secular variation of Earth magnetism in Plio–Pleistocene basalts of eastern Iceland. Geol. Mijnbouw 43, 403–413.

Wensink, H., 1964b. Paleomagnetic stratigraphy of younger basalts and intercalated Plio–Pleistocene tillities in Iceland. Geol. Rundsch. 54, 364–384.

Wilson, R.L., 1970. Permanent aspects of the earth's non-dipole magnetic field over upper tertiary times. Geophys. J. R. Astron. Soc. 19, 417–437.

Zijderveld, J.D.A., Hilgen, F.J., Langreis, C.G., Verhallen, P.J.J.M., Zachariasse, W.J., 1991. Integrated magnetostratigraphy and biostratigraphy of the upper Pliocene–lower Pleistocene from the Monte Singa and Crotone areas in Calabria, Italy. Earth Planet. Sci. Lett. 107, 697–714.